Nested piezoelectric cellular actuators for a biologically inspired camera positioning mechanism

Joshua Schultz, Jun Ueda, *Member, IEEE,*

Abstract—Using successive stages, or nesting compliant amplification mechanisms, soft actuators with performance suitable for robotic applications can be constructed with piezoelectric ceramic as the active material. This paper presents a mathematical framework that describes the interactions among the various amplification mechanisms in a hierarchical nested structure. A formal treatment of nested amplification mechanisms results in two theorems that describe the stiffness properties of the whole actuator in terms of the properties of each mechanism in the hierarchy. These theorems show that the stiffness properties of the actuator can be computed by considering only the outermost few layers in the nested configuration. By virtue of this hierarchical structure, the actuator also assumes a cellular structure; it functions by summing the effects of on-off inputs coupled by a flexible connective medium. This requires a paradigm shift when selecting control strategies. A multi-layer strain amplification mechanism is designed to meet the required range of travel for a biologically inspired camera positioning mechanism, and a switching control method for the actuator's 16 on-off inputs are discussed.

Index Terms—compliant mechanisms, biologically inspired systems.

I. INTRODUCTION

Soft actuators have been an important focus in robotics in recent years. They have been shown to have promise in numerous fields, such as haptics [1] and rehabilitation robotics [2]. This paper demonstrates the use of "amplified" actuators, whereby an active material, such as a piezoelectric ceramic, acts through a compliant mechanism to orient a camera [3], shown in Figure 1. The compliant mechanism increases the stroke compared to that of the active material itself, sacrificing greater-than-needed force capability.

Not only does the amplification mechanism produce a more convenient stroke-force operating characteristic from an otherwise lackluster active material, it also naturally introduces compliance into the actuator with no need for a dedicated part. The camera positioning mechanism then has a muscle-like quality in that it has a compliant medium between the load and the active material [4]. The amplification is accomplished in several nested stages, with each stage amplifying the output of numerous lower-level sub-units, with the active material constituting the lowest-level subunit in the hierarchy. The multi-stage nested mechanism is necessary because geometric constraints render it impossible to achieve the aggressive force-displacement tradeoffs required by robotic devices using only a single stage. Because the actuator contains multiple

Joshua Schultz received his Ph.D. from the George W. Woodruff School of Mechanical Engineering, Georgia Institute of Technology, Atlanta, GA, 30332 USA in 2012, and Jun Ueda is with the George W. Woodruff School of Mechanical Engineering, Georgia Institute of Technology, Atlanta, GA, 30332 USA e-mail: joshua.schultz@gatech.edu.
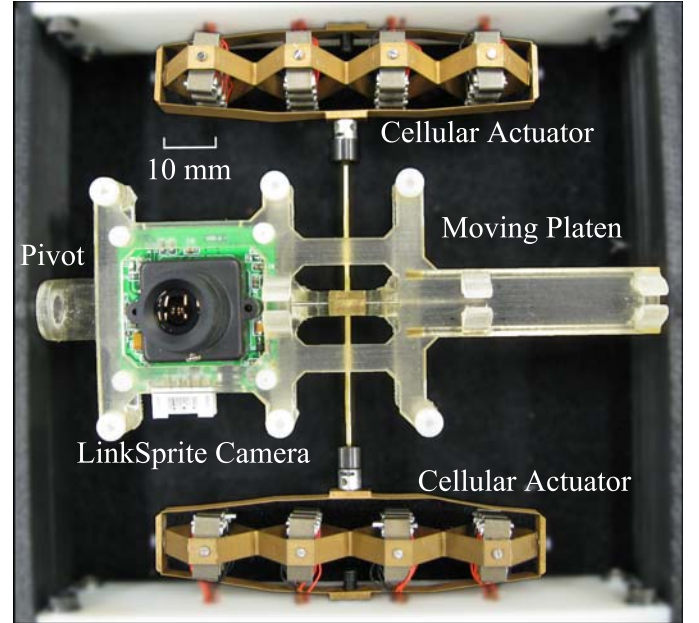

Fig. 1. Camera driven by an antagonistic pair of piezoelectric cellular actuators

active units, it exhibits a second muscle-like quality, that of a *cellular structure*, or the idea that motion is accomplished by coordinating on-off activation of distinct motor units. The two-port network formalism from circuit theory provides the necessary abstraction to describe the interconnections between these various amplification stages in a simple, tractable manner. Using this formalism, it is a simple matter to compute performance metrics from the characteristics of the individual layers.

In fact, measurements of human saccadic eye motions show that the neuronal pulse amplitude does not vary greatly with the length of the move, rather it is the duration of the pulse that is the driving factor and the control inputs are of the bang-bang type [5]. The cellular structure of the camera positioning mechanism, which can only apply impulsive inputs, also falls within this paradigm.

The engineering goals inherent in producing a camera positioning mechanism with actuation performance comparable to human recti muscles give rise to two important research questions. First, as the amplification stages are connected together, how are the overall properties of the actuator connected to the properties of its component parts? Considering this in a formal, systematic way, this paper reveals two "nesting theorems" that confirm an intuitive result, namely that the stiffness observed by the environment depend most strongly

on the outermost layers in the hierarchy: those closest to the load. It is these layers that should receive the most attention in the design and manufacturing process if actuator stiffness is of primary concern. These theorems were presented in an abbreviated form in [6]; this article contains the complete proofs and experimental evaluations that did not appear in the prior work. Secondly, how can the various active units within the actuator be coordinated in an efficient manner to produce smooth motion? The compliant nested configuration sums the contributions of various "motor units" to achieve a desired overall effect much in the way that connective tissue in human muscles does. For this reason, we apply discrete switching vibration suppression (DSVS) [7] to move the device smoothly. Although physiological literature and empirical evidence [5] strongly suggest that the human eye is driven by impulsive inputs, existing camera positioning mechanisms in the literature are neither actuated nor controlled in this way. The cellular structure and DSVS control architecture make this positioner the first of its kind to bear semblance to the human eye in this way.

The multi-stage mechanism (3 stages in the example fabricated here) will produce an aggressive force-displacement tradeoff on the bare piezoelectric stack's performance, producing a truly compliant muscle-like actuator with no stick-slip elements, in contrast to other examples in the literature. Recent works have recognized the drawbacks inherent in traditional motor-on-motor camera positioner designs (namely that the inertia of the actuators is larger than that of the camera itself) and have proposed novel systems with better performance.

Villgrattner and Ulbrich [8] present a mechanism that uses ultrasonic motors. The stick-slip actuators they use lack the natural compliance found in human muscle, however. Lee, et. al. [9] recognize the important role compliance plays in the motion of the human eye and introduce deformable connecting beams in lieu of rigid connecting rods. The actuation effort is produced by stepper motors. Unlike these two solutions, the amplified piezoelectric technology represents a highly integrated, compliant interaction with the environment that has much more in common with human recti muscles.

Use of piezoelectric ceramics together with amplifying mechanisms in the robotics context has been primarily restricted to end effectors, such as the gripper of Huang and Chen [10]. The typical approach, as summarized by Kota, et al. [11], is to begin with a mesh-like ground structure and use an automated process to do a topological optimization based on the task. Once the optimal connectivity is determined, a size and shape optimization process follows, where geometric constraints such as minimum thickness can be imposed. While this is an effective method of designing special purpose devices, it is not particularly effective in producing general-purpose actuation, i.e. compliant muscle-like actuators to drive robotic links. In addition, to the authors' knowledge, devices of this type are exclusively planar, and therefore do not represent the best use of space.

Some more general-purpose and more modular methods of amplifying piezoelectric ceramic output are described by Uchino [12], and go by trade names such as "moonies" or "rainbows." The smart structures literature contains a number of excellent theoretical and experimental works on devices of these types; notable examples include the seminal work of Paros and Weisbord on the analysis of flexure hinges [13], and Lobontiu and Garcia [14], who optimize a flexure hinged mechanism with respect to a cost function trading off geometric advantage and efficiency. A common thread among mechanisms of this type is that they are longer in the input direction (corresponding to the piezoelectric stack's longitudinal direction) than in the output (or actuation) direction.

The remainder of the paper will be organized as follows: Section II will introduce some key concepts particular to compliant actuators with a cellular structure. Sections III-VII detail the theoretical results that emerge from the two-port formalism. Sections VIII and IX will present experimental measures of the actuator performance. Section X will discuss control for vibration-free point-to-point motion that is compatible with the actuator's cellular structure.

II. FROM PIEZOELECTRIC STACKS TO MUSCLE-LIKE ACTUATORS

A. A large-strain compliant actuator

Although "moonies" and their brethren can increase the displacement by an order of magnitude (over that of the piezoelectric stack alone), *it is still to small to be useful in robotics applications*. Combining enough of these in series can reach the required stroke, but the total length of the series chain will be too long to be useful. For this reason, several researchers have pursued the idea of *nested* amplification mechanisms, where the overall amplification is accomplished in successive stages or *layers*. Figure 2 illustrates this diagrammatically. In actuators of this type, the output of series-parallel chains of an amplified active material serves as the input to the subsequent amplification mechanism. There are three major advantages to this: first, the amplification factor of a single mechanism is limited by geometric and kinematic constraints, and multiple stages can allow the amplification to proceed further. Second, the device can be constructed so that each layer is mutually orthogonal to the previous and subsequent layers. As increased performance is required, the actuator is able to grow in any of the three dimensions of space, and will be less likely to violate the required envelope than would planar mechanisms for the same performance requirement. Third, with multiple layers, it is conceivable that multiple configurations exist that would meet the desired force-displacement tradeoff, and this additional design freedom could be used to meet additional criteria, such as an improved frequency response.

Given the apparent benefits of three-dimensional multistage designs, it is worthwhile to find systematic ways of specifying and producing these mechanisms despite the added complexity. The works that do present some sort of three-dimensional or multi-stage compliant amplification mechanism [15]–[18] provide no rationale for their nested design other than to say that a single amplification mechanism produced insufficient displacement. Neither do they provide a general mathematical description that describes the behavior of multi-layer nested structures across a wide range of geometries and over travel. Structures such as these quickly become difficult to analyze
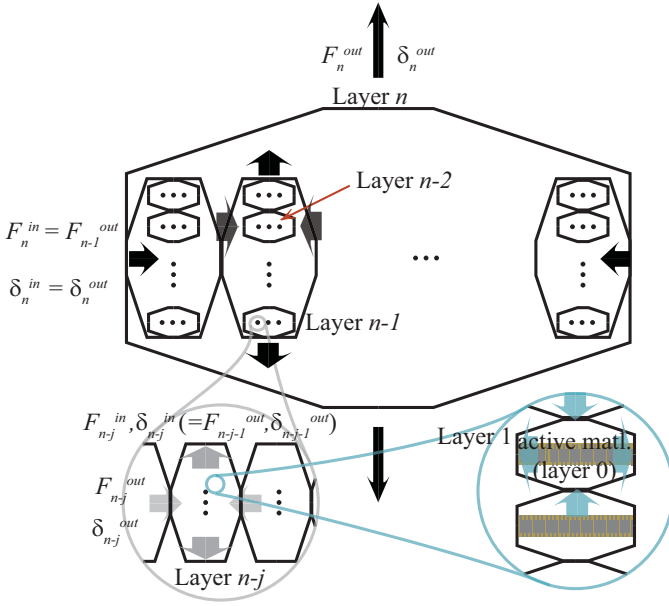
Fig. 2. Diagrammatic construction of a hierarchical nested strain amplifying mechanism. The term *nested* is used because each stage is typically placed inside the subsequent stage. The force and displacement produced by each stage serves as the input to the next.
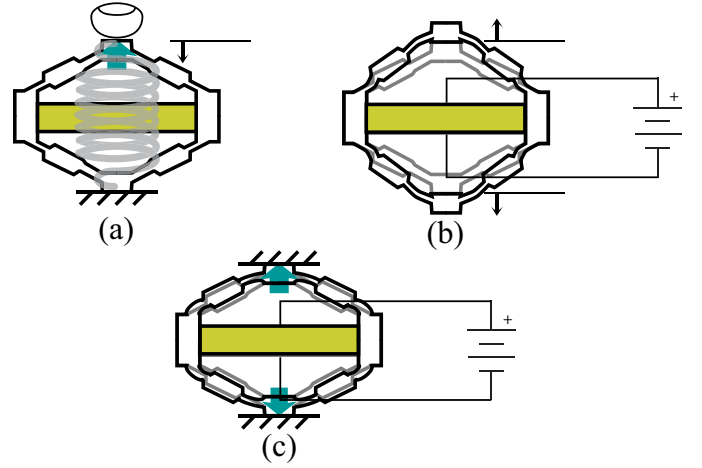

Fig. 3. Performance metrics for compliant actuators: (a) stiffness viewed from the environment, (b) free displacement at maximum activation, (c) blocked force at maximum activation

using traditional methods, even for small numbers of layers. As the number of layers becomes large, numerical techniques, such as finite element methods, can become unworkable because of the multiply connected topology and the difficulty meshing the structure due to interfaces and differences in characteristic dimension between the layers. In addition, the robotics community is primarily interested in input-output behavior, not internal forces and nodal displacements, meaning that a lot of computational power is wasted on calculating information that is not used. For this reason, this work explores the input-output characteristics of actuators using this nested strain amplification architecture, and presents an abstraction that simplifies and partitions the analysis, producing an elegant description of the behavior of these kinds of actuators even with a large number of layers.

B. Performance Metrics

Amplified piezoelectric stacks are unlike servomotors in several respects. Most importantly, their force is not constant with stroke, but decreases with displacement. This is consistent with biological actuation systems. There are 3 natural metrics associated these types of actuators, illustrated in Figure 3. The first (a) is the stiffness of the de-energized actuator as perceived by another device or entity in the environment in contact with the actuator's output. The second (b) is the free displacement, or the maximum displacement achieved when the actuator is energized. The third (c) is the blocked force, or the force applied to the load when the load prevents the actuator from moving. This is equivalent to an isometric contraction in muscle. The amount of force the actuator can impose on the driven load decreases linearly with position, from the blocked force at zero displacement, to a value of zero at the free displacement.

C. Antagonistic connections

The camera positioning mechanism shown in Figure 1 is driven by means an antagonistic pair of piezoelectric cellular actuators, which in effect function like a pair of recti muscles in the human eye [19]. Like biological actuation systems, these actuators can only contract in response to a command, not extend. Also like human muscles, they present a compliant interface with the environment and function by means of discrete actionable units. The camera positioner has a range of motion similar to the human eye, with high bandwidth; it can easily move at speeds exceeding 7 Hz.

Figure 4 shows an oblique view of one of the actuators so that all of its parts are visible. The actuator contains 16 active units, which can be activated independently in an on-off manner only. Different levels of activation will cause the actuator to contract, as illustrated. Each piezoelectric stack is inside of a rhomboidal strain amplifying mechanism; this is the first stage (or "layer") of amplification in the hierarchy. The piezoelectric stack plus rhomboidal mechanism, a single-stage amplification device that makes up this "first layer" is commercially available from the Cédrat corporation (Model APA50XS). A serial chain of 4 of these units is placed inside another rhomboidal strain amplifying mechanism (the second layer), and 4 of these "second-layer units" are placed in the outermost strain amplifying mechanism, which accomplishes the final stage of the force-displacement tradeoff. This is representative of the entire class of multi-stage amplifying mechanisms discussed in this paper.

Consider a mechanism driven by two identical multi-stage amplified actuators in the absence of any external load, with no preload at the neutral position, such as the camera positioner shown in Figure 1. Each actuator consists of m piezoelectric stacks with n layers of amplification. To achieve some desired position, one of the cellular actuators (henceforth called the "active" actuator) will be energized, and will contract. The remaining actuator (the "passive" actuator) will not be energized, but will, due to its inherent stiffness, oppose the motion of the active actuator, stopping it short of its free displacement.
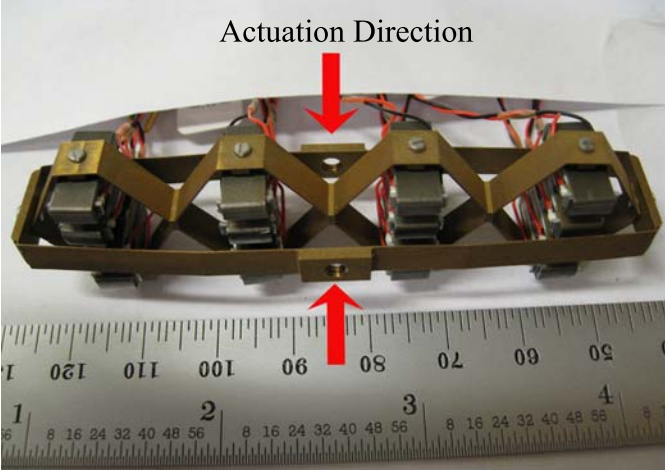
Fig. 4. Three layer nested strain amplified piezoelectric actuator used in the camera positioning mechanism

The antagonist pair configuration and the resulting motion is illustrated in Figure 5 and also in the companion video. Using a two-port network framework [20] and assuming the material properties and terminating electrical impedance characteristics of the piezoelectric stack are known, it is possible to predict the maximum displacement of the antagonistically driven device.

III. TWO-PORT MODELS OF STRAIN AMPLIFYING MECHANISMS

The amplification mechanism of each layer can be described by a two-port network model, an intellectual device taken from circuit theory that concisely describes input-output behavior while abstracting away internal variables [20]. Abdalla, et al. [21] used two-port networks to optimize a planar compliant mechanism for a known load and to describe the electro-mechanical transduction of a piezoelectric stack. The mathematical relationship between the input and output to the mechanism is described by the following:

$$\left[\begin{array}{c} F^{in} \\ F^{out} \end{array} \right] = \left[\begin{array}{cc} s_1 & s_3 \\ s_3 & s_2 \end{array} \right] \left[\begin{array}{c} \delta^{in} \\ \delta^{out} \end{array} \right], \qquad (1)$$

where F^{in}, F^{out}, δ^{in} and δ^{out} denote the forces and displacement at the input and output ports, respectively. s_1, s_2, and s_3 have units of stiffness and are functions of the geometry and material properties. Using this modeling technique for rhomboidal strain amplifying mechanisms assumes that the material is linearly elastic and undergoes small changes in angle. This is valid for the piezoelectric cellular actuator because the outermost layers tend to have small angle values, and the innermost undergo smaller motions by virtue of the fact that their displacements are being amplified by subsequent stages. A procedure to determine these quantities for rhomboidal mechanisms is described in [22]. The matrix in (1) is the stiffness matrix, one of several *immittance* matrices [20] that is used to describe the two-port network relationship. The strength of the two-port network approach is that it accurately accounts for the effects of both the control force applied by previous layers and environmental or load forces

(a) Pictorial representation of the camera mechanism

(b) Actuator flexed   (c) Actuator extended

(d) Camera at extreme left   (e) Camera at extreme right

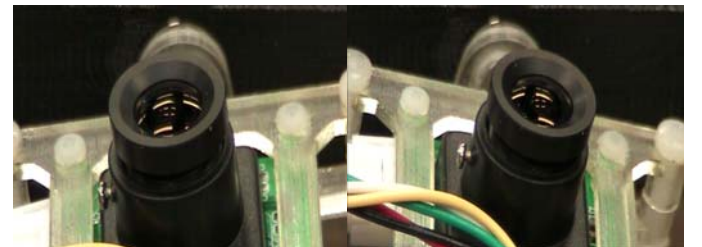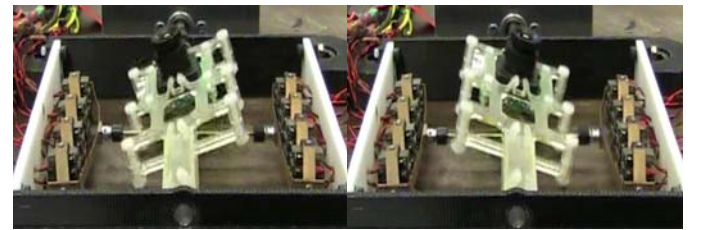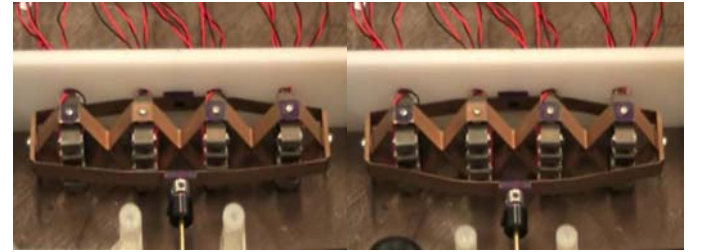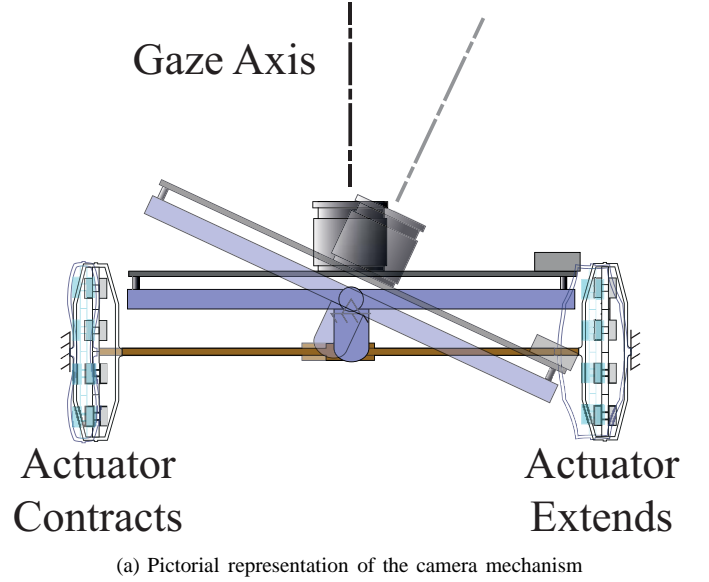(f) Closeup of camera pointing left   (g) Closeup of camera pointing right

Fig. 5. Camera positioner driven by an antagonist pair. The active actuator will contract, but its action is opposed by the stiffness of the passive actuator on the other side.
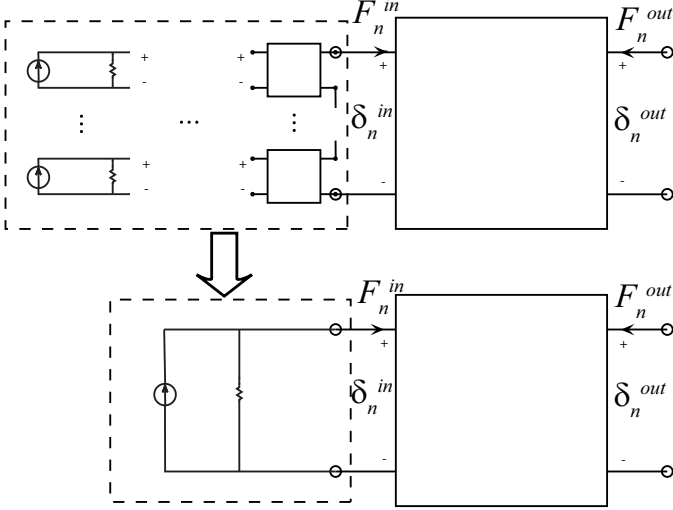
Fig. 6. Collapsing of two-port networks. Each square box represents a two-port network, with a voltage and current at the right and left hand ports. The entire hierarchy within the dashed lines is collapsed and replaced with its Norton circuit.

from subsequent layers. Using this framework, it is possible to model systems that do not have the high input impedance/low output impedance characteristics necessary in most branches of circuit analysis. An alternate way of expressing this is to say that the two-port (or multiport) network succeeds in modeling devices that have significant "back effects."

The innermost, or "zeroth," layer of a nested cellular device will be some active material of known characteristic. Typically the manufacturer tabulates the totally blocked, or clamped, force and the mechanical stiffness. This can be represented as a Norton equivalent circuit, where the blocked force is represented by a current source, and the mechanical stiffness is represented by the Norton resistance. The displacement of this device, which is analogous to the voltage across the Norton resistance, will depend on the load impedance. Several of these zeroth layer units can be combined in series, and their Norton circuits combined according to the methods of circuit analysis. The voltage across the Norton equivalent resistance corresponds to the input displacement of the first layer displacement amplification mechanism. The current to the load impedance corresponds to the input force. When the amplification mechanism is represented as a two-port network, this is the voltage and current at the left hand port. With appropriate mechanical analogies, this can be expressed as:

$$F_1^{in} = F_0^{block} - k_0 \delta_1^{in} \qquad (2)$$

Because series combinations of springs add compliances, not stiffnesses, the Norton equivalent resistance is set to $1/k_0$. Interconnections between networks are described in terms of matrix operations on the immittance matrices and are well known [20]. Therefore any combination of two-port networks can be readily analyzed. The topological relationships between the various layers in the hierarchy will be represented by the electrical connections of their two-port models.

IV. COLLAPSING OF NESTED TWO-PORT MODELS

Since the impedance characteristic at the input to the first amplification layer is known, and the immittances of the amplification mechanism's two-port model are known, the entire connection can be "collapsed" and replaced with the Norton equivalent circuit that represents the characteristic at the output of the first layer. This can be performed repeatedly, up to the outermost layer, which is connected to the load. Figure 6 illustrates collapsing connections of two-port networks. If the input to a given amplifying mechanism is a series combination of subunits, as it is in the camera positioner application, this can be mathematically represented by replacing the series combination with a fictional unit with the same blocked force and stiffness as the series combination. The following derives the equations that describe the collapsing process.

Consider an active material with blocked force F_0^{block} and stiffness k_0. The output of this Norton circuit is applied to the left hand port of a two-port network representing the first layer amplification mechanism. The displacement of the zeroth layer, δ_1^{in}, is analogous to the voltage across the Norton resistance. Using (2) and (1) the two-port relationship can be represented by the following equation:

$$\left[\begin{array}{c} F_0^{block} - k_0 \delta_1^{in} \\ F_1^{out} \end{array} \right] = \left[\begin{array}{cc} s_1 & s_3 \\ s_3 & s_2 \end{array} \right] \left[\begin{array}{c} \delta_1^{in} \\ \delta_1^{out} \end{array} \right] \qquad (3)$$

Solving the upper of the two equations for δ_1^{in}, we get

$$\delta_1^{in} = \frac{F_0^{block} - s_3 \delta_1^{out}}{s_1 + k_0} \qquad (4)$$

Substituting this into the lower of the two equations and collecting terms we obtain:

$$F_1^{out} = \frac{s_3 F_0^{block}}{s_1 + k_0} + \frac{s_2(s_1 + k_0) - s_3^2}{s_1 + k_0} \delta_1^{out} \qquad (5)$$

Defining the following:

$$F_1^{block} = \frac{s_3 F_0^{block}}{s_1 + k_0} \qquad (6)$$

$$k_1 = \frac{s_2(s_1 + k_0) - s_3^2}{s_1 + k_0} \qquad (7)$$

Equation (5) can be written as:

$$F_1^{out} = F_1^{block} + k_1 \delta_1^{out}. \qquad (8)$$

This has physical significance; F_1^{block} is the fully blocked force of the displacement amplified active material, and $k_1 \delta_1^{out}$ is the stiffness as seen from the output of the combination times the output displacement of the compliant mechanism. Since this is an equivalent stiffness for the nested connection, we refer to it as the *lumped stiffness*. In the Norton equivalent circuit, F_1^{block} corresponds to the current source and $\frac{1}{k_1}$ corresponds to the equivalent Norton resistance. This procedure can be performed repeatedly for each amplification mechanism in the hierarchy.

V. DISPLACEMENT OF THE MECHANISM AGAINST THE PASSIVE ACTUATOR

Modeling the camera platen as a rigid body that rotates about a frictionless pivot, neglecting acceleration, and representing the antagonistic pair as a connection of two-port models results in the configuration shown in Figure 7. From this model, we see that the following relations hold:

$$\delta_{active}^{out} = -\delta_{passive}^{out} \tag{9}$$

$$F_{active}^{out} = F_{passive}^{out} \tag{10}$$

where $\delta_{active}^{out}, \delta_{passive}^{out}, F_{active}^{out}, F_{passive}^{out}$ are as shown in Figure 7. Let us assume that the antagonistic actuators are identical. Because the passive actuator is off, the current source F_0^{block} will be zero. The stiffness k_0 at the zeroth layer of the passive actuator will depend on the electrical terminating impedance on the leads of the active material. It will be shown later that the effect of the terminating impedance on the stiffness is minimal.

Because the passive actuator is not energized, it can be completely collapsed and simply be represented as a terminal resistance $\frac{1}{k_{eq}}$ across the active actuator. This is illustrated in Figure 7. The displacement of the antagonistic mechanism corresponds to the voltage across the right hand port of the two-port model of the outermost layer of the active actuator.

Using (3) and Ohm's law, solving for δ_n^{out} we get:

$$\delta_n^{out} = -\frac{s_3 F_{n-1}^{block}}{s_1 s_2 - s_3^2 + k_{eq}(s_1 + k_{n-1}) + s_2 k_{n-1}}. \tag{11}$$

The free case has $k_{eq} = 0$ resulting in a displacement of:

$$\delta^{free} = -\frac{s_3 F_{n-1}^{block}}{s_1 s_2 - s_3^2 + s_2 k_{n-1}}. \tag{12}$$

Taking the ratio of the two gives:

$$\frac{\delta_n^{out}}{\delta^{free}} = \left(1 + \frac{k^{out}(s_1 + k_{n-1})}{s_1 s_2 - s_3^2 + s_2 k_{n-1}}\right). \tag{13}$$

Assuming that the electrical terminating impedance on the passive side is chosen so as to have the same mechanical stiffness for the zeroth layer as on the active side, using (6) we can write:

$$k^{out} = \frac{s_2(s_1 + k_{n-1}) - s_3^2}{s_1 + k_{n-1}}. \tag{14}$$

substituting into (13) we get $\delta_n^{out}/\delta^{free} = 1/2$. Therefore, in an antagonistic pair, the actuator must be designed so that its free displacement is double the stroke length corresponding to the angle of travel specification.

VI. NESTING OF LAYERS

If a passive actuator is in an antagonistic pair arrangement with an active actuator, it will appear to the active actuator as a stiffness. This stiffness will depend on the immittances of previous layers, as well as the terminal stiffness of the zeroth layer. This section will consider an amplified mechanism with

n layers, with outermost layer (connected to the load) denoted layer n. The innermost layer (connected to the active material) will be denoted layer 1. Immittances for a given layer will be denoted with a leading superscript. k will be used to count layers outward from the active material, and $j \in \mathbb{N} \mid n - j \in [0, k]$ will be used to count layers inward from outermost. The stiffness of a passive actuator with n layers is

$$k_{passive} = {}^n s_2 - \cfrac{{}^n s_3^2}{{}^n s_1 + {}^{n-1} s_2 - \cfrac{{}^{n-1} s_3^2}{{}^{n-1} s_1 + {}^{n-2} s_2 - \cfrac{{}^{n-2} s_3^2}{{}^{n-2} s_1 + {}^{n-3} s_2 - \ddots}}}. \tag{15}$$

For the jth layer, denoting

$$^j\gamma = {}^{n-j} s_2 - \frac{{}^{n-j} s_3^2}{{}^{n-j} s_1 + k_{n-j-1}} \tag{16}$$

where k_{n-j-1} is the lumped stiffness of the $j - 1st$ layer subunit and subsumes all terms for any nested unit index (numbered from the outside in) $i > j$, we can state that

$$-\frac{{}^{n-j} s_3^2}{{}^{n-j} s_1} < {}^{j-1}\gamma - {}^{n-j} s_2 < 0. \tag{17}$$

Therefore, approximating the stiffness of the passive actuator by truncating remaining terms in the denominator will result in a conservative estimate of the displacement for a nested structure.

VII. ESTIMATING STIFFNESSES OF ACTUATORS WITH LARGE NUMBERS OF LAYERS

Equation (15) has a form of a continued fraction. This results in some desirable properties. The following section will show that for an actuator with a large number of layers, the stiffness of the entire actuator can be approximated to a desired degree of accuracy by replacing the continued fraction representing the remaining ayers by an arbitrary constant. In the literature [23], [24], these approximations are known as *convergents*.

We intend to show that the sequence of convergents P_j is Cauchy, and therefore, all convergents beyond some finite k lie within some interval of size ϵ of P_k on $\mathbb{R}$.

Lemma 1. *All denominators for the continued fraction expansion of the stiffness of a nested linearly elastic mechanism are positive.*

Proof: Each compliant mechanism has a positive definite immittance matrix. Therefore, the determinant for any layer, $^k s_1^k s_2 - {}^k s_3^2 > 0$. Because any realizable nested actuator will contain a finite number of compliant mechanisms, the continued fraction expansion terminates. Let us refer to the sequence of continued fraction expansions for the lumped stiffness at the output of each layer, beginning with the innermost, as z_k. The zeroth term of the sequence, z_0 is
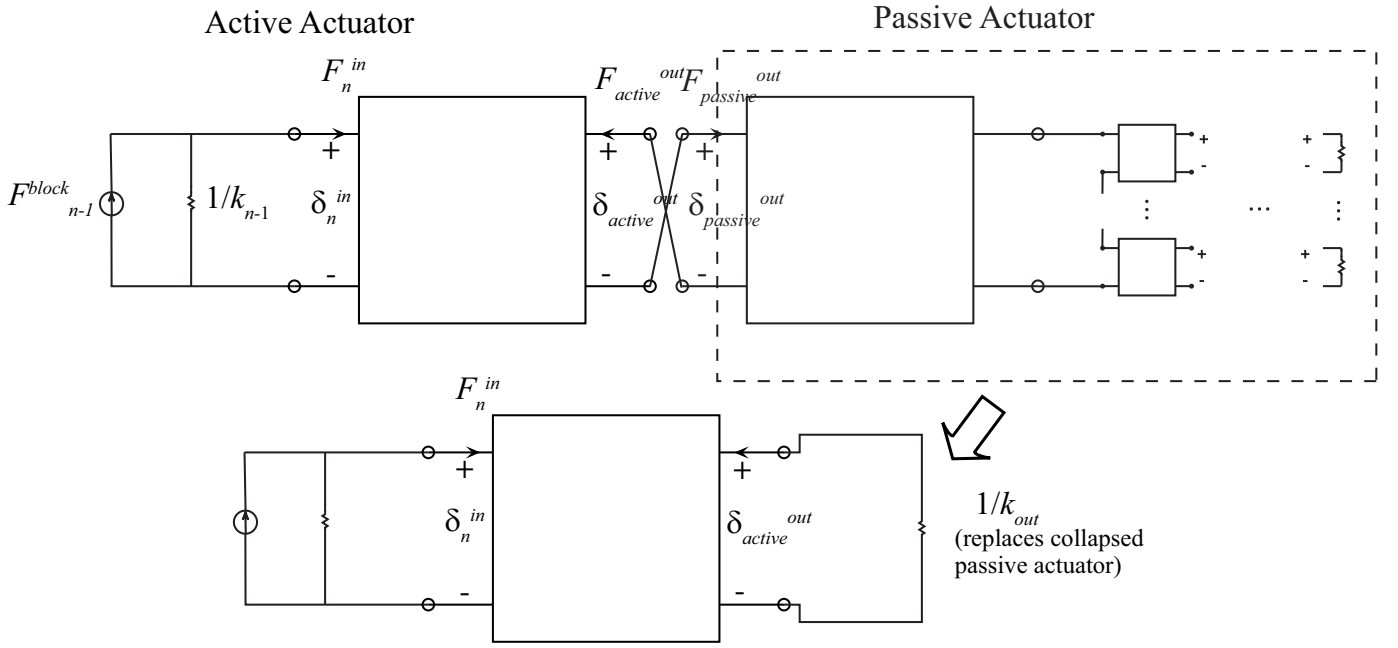
Fig. 7. Two port representation of antagonistic pairs. The active actuator is in black and has all but the outermost layer collapsed and represented by its Norton circuit. The passive actuator is in gray and is will be replaced by a simple stiffness)

constant. Because the stiffness is derived from passive elastic material, z_0 will be positive, and all elements of the immittance matrix are positive. We can express the remaining terms of the sequence by the recursive relation:

$$z_k = {}^k s_2 - \frac{{}^k s_3^2}{{}^k s_1 + z_{k-1}} \tag{18}$$

This can be rewritten as

$$z_k = \frac{{}^k s_2 {}^k s_1 - {}^k s_3^2 + {}^k s_2 z_{k-1}}{{}^k s_1 + z_{k-1}} \tag{19}$$

If $z_{k-1} > 0$, $z_k > 0$. The proof is completed by induction on k. ∎

When a force is applied at the output of a compliant mechanism, it not only causes a deformation in the output direction; it causes a deformation in the input direction as well. This deformation at the input has an effect equivalent to a force transmitted back to the output, even when no load is applied at the input. Essentially, Lemma 1 says the effective stiffness due to this back, then forward transmission, s_3^2/s_1 will always be less than the input clamped output stiffness, s_2.

Lemma 2. *In the set of all terminating continued fractions of*

the form:

$$\begin{cases} p_k = a_0 - \cfrac{b_1}{a_1 - \cfrac{b2}{a_2 - \cfrac{b3}{\ddots \cfrac{}{a_{k-1} - \cfrac{b_k}{c_k}}}}} \\ \mid a_i, b_i > 0 \; \forall i, c_k \in \left(\frac{b_k}{a_{k-1}}, \; c_{max} \right] \end{cases} \tag{20}$$

with a_i, b_i constant the maximum p_k is achieved by choosing the maximum c_k, c_{max}.

Proof: For $k = 1$, $p_k = a - \frac{b}{c}$. It is clear that this quantity is maximized by the largest possible c. For the general case: define the quantity $a_{k-1} - \frac{b_k}{c_k} = c_{k-1}$. c_{k-1} is maximized by $c_k = c_{max}$. Therefore, by induction, choosing the maximum c_k maximizes all denominators, and p_k is maximized. ∎

This is equivalent to saying that the stiffest possible actuator can be realized by clamping the input of the innermost mechanism.

Theorem 1. *The sequence of convergents of the continued fraction expansion of the stiffness of a nested mechanism, with successive denominators for $n-j < k$ replaced by ${}^{k-1}s_1 + {}^k s_2$ is Cauchy.*

Proof: Any continued fraction can be represented by

$$p_n = {}^n s_2 - \cfrac{{}^n s_3^2}{{}^n s_1 + {}^{n-1} s_2 - \cfrac{{}^{n-1} s_3^2}{{}^{n-1} s_1 + {}^{n-2} s_2 + \cfrac{\ddots}{{}^{n-j+2} s_1 + {}^{n-j+1} s_2 - \cfrac{{}^{n-j+1} s_3^2}{{}^{n-j+1} s_1 + z_j}}} \tag{21}$$

Equation (21). This considers the denominators from the top level, n, down to level $n-j$; z_j represents the continued fraction expansion for the remaining layers. It can be approximated by:

$$z_j \approx {}^{n-j} s_2 - \frac{{}^{n-j} s_3^2}{{}^{n-j} s_1 + {}^{n-j-1} s_2}. \tag{22}$$

Let y_j represent the convergent 21 where z_j is replaced by the approximation in (22). Physically speaking, this represents the stiffness perceived at the output when the innermost layer considered in the approximation (layer j) has its input fixed. Accordingly, y_j has units of stiffness. y_{j-1} represents the previous convergent in the sequence, replacing the final z_j simply by ${}^{n-j} s_2$. By lemma 1, the quantity $\frac{{}^{n-j} s_3^2}{{}^{n-j} s_1 + z_j}$ will be positive for all j. Also from lemma 1, it can be determined that this quantity will not exceed ${}^{n-j} s_2$. y_{j-1} and y_j are identical, except for the terminating constant. Therefore, they are both of the form of the continued fraction in lemma 2. y_{j-1} terminates with the constant $c_k = {}^{n-j+1} s_1 + {}^{n-j} s_2$ and y_j terminates with the constant $c_k = {}^{n-j+1} s_1 + {}^{n-j} s_2 - \frac{{}^{n-j} s_3^2}{{}^{n-j} s_1 + {}^{n-j-1} s_2}$. By lemma 2, and induction on j, we can say the sequence of convergents is monotonically decreasing, or

$$y_{j-1} > y_j \ \forall j. \tag{23}$$

Applying lemma 1 at level n, we can say the sequence is bounded below by 0. Since the sequence is monotonically decreasing and bounded below, it must be Cauchy. ∎

For any Cauchy sequence, for any arbitrary ϵ, we can find a k such that all terms in the sequence beyond k are within a distance ϵ from one another [25]. Physically speaking, this means that for an actuator consisting of nested compliant mechanisms, we can approximate its stiffness to some desired accuracy by considering merely the outer k layers and considering the lumped stiffness of the $k-1^{st}$ layer to be infinite. Alternatively, the kth layer can be said to be clamped at its input.

Theorem 1 says that outer layers, regardless of whether they are rigid or compliant, have the greatest effect on the stiffness of the overall actuator. Therefore, the innermost layers do not need to have as strict tolerances as the outermost layers to achieve a uniform stiffness from actuator to actuator. It also means that the electrical terminating impedance of the passive actuator is not critical for actuators with large numbers of layers, justifying the assumption in Section V. The procedure of Theorem 1 provides an upper bound on the true stiffness.

An alternate choice is to approximate z_j by ${}^{n-j} s_2 - \frac{{}^{n-j} s_3^2}{{}^{n-j} s_1}$. The sequence of these approximants (which are not convergents, strictly speaking, since they do not result from a strict truncation) will be denoted by x_j. Like y_j, this has units of stiffness This is equivalent to the stiffness perceived at the output when the innermost mechanism considered in the approximation is free to deform in the input direction. It will be shown that y_j and x_j have the same limit.

Theorem 2. *The sequences y_j and x_j converge to the same limit.*

Proof: Any continued fraction of the form in Lemma 2 can be represented by the recursive relation:

$$\begin{aligned}
B_{j+1} &= a_{j+1} B_k - b_{j+1} B_{j-1} \\
A_{j+1} &= a_{j+1} A_k - b_{j+1} A_{j-1} \\
y_{j+1} &= \frac{B_{j+1}}{A_{j+1}} \\
B_{-1} &= 1 \\
B_0 &= a_0 \\
A_{-1} &= 0 \\
A_0 &= 1
\end{aligned} \tag{24}$$

This is shown in Rockett and Szüsz [24]. In this case $a_{j+1} = {}^{n-j+1} s_1 + {}^{n-j} s_2$ and $b_{j+1} = {}^{n-j+1} s_3^2$. Using a similar procedure, it is simple to demonstrate that x_{j+1} can be written as:

$$x_{j+1} = \frac{B_{j+1} - k_{j+1} B_j}{A_{j+1} - k_{j+1} A_j} \tag{25}$$

where $k_{j+1} = \frac{{}^{n-j} s_3^2}{{}^{n-j} s_1}$. Note that each term of x_j is written in terms of the B_j, A_j used to construct y_j. We then construct the sequence $y_j - x_j$ and show that it approaches zero in the limit. After algebraic manipulations, the $j+1^{st}$ term of the sequence can be written as:

$$y_{j+1} - x_{j+1} = \frac{y_j - y_{j+1}}{\frac{A_{j+1}}{k_{j+1} A_j} - 1}. \tag{26}$$

The numerator approaches zero for large j by Theorem 1. To show that the entire sequence goes to zero it is sufficient to show that $\frac{A_{j+1}}{A_j} \neq k_{j+1}$. This can be proved by contradiction.

Assume that for all j greater than some k the sequence $\frac{A_j}{A_{j-1}} = k_j$. Then $\frac{A_{j+1}}{A_j} = k_{j+1}$. This can be rewritten as:

$$A_{j+1} = k_{j+1} A_j = a_{j+1} A_j - b_{j+1} A_{j-1}. \tag{27}$$

collecting terms and substituting in the immittances we get:

$${}^{n-j} s_3^2 A_{j-1} = \left({}^{n-j} s_1 + {}^{n-j-1} s_2 - \frac{{}^{n-j-1} s_3^2}{{}^{n-j-1} s_1} \right) A_j. \tag{28}$$

(a) Convergence of input fixed (y_j) and input free (x_j) approximations
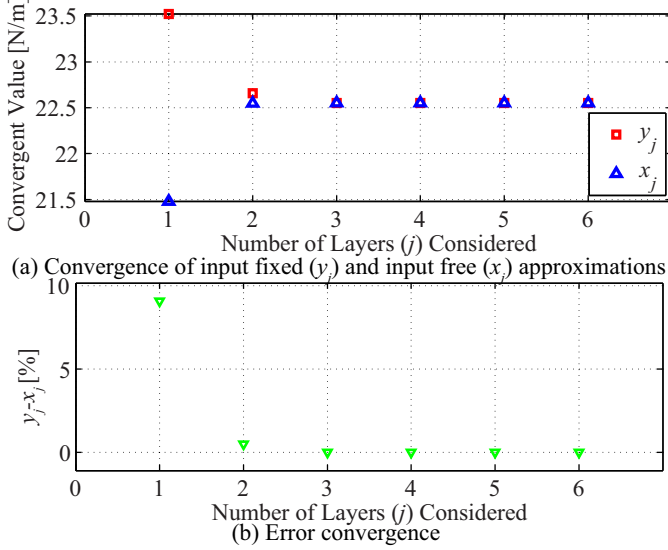
(b) Error convergence

Fig. 8. Convergence of the various stiffness approximations for a hypothetical many-layered mechanism with randomly chosen immittances. y_k is the input-fixed approximation through layer k, and x_k is the input-free approximation.

Fig. 9. Experimental evaluation of y_0 (input-fixed stiffness of the outermost layer only)

We can divide this quantity by A_{j-1}. Since j is assumed to be greater than k, the sequence $\frac{A_j}{A_{j-1}} = k_j$. Substituting in for this quantity in terms of the immittances we get:

$$^{n-j}s_3^2 = \frac{^{n-j}s_3^2}{^{n-j}s_1}\left(^{n-j}s_1 + ^{n-j-1}s_2 - \frac{^{n-j-1}s_3^2}{^{n-j-1}s_1}\right). \quad (29)$$

Simplifying, we get:

$$\frac{^{n-j-1}s_2 \, ^{n-j-1}s_1 - ^{n-j-1}s_3^2}{^{n-j-1}s_1 \, ^{n-j}s_1} = 0. \quad (30)$$

All $^k s_i$ are finite, and the numerator of (30) is simply the determinant of the immittance matrix for layer $n-j-1$. This must be strictly positive for all j, hence the contradiction and the result is proved. ∎

A simple numerical example of the convergence is shown in Figure 8. Figure 8 (a) shows the convergence rates of the input-fixed and input-free approximations y_j and x_j, and Figure 8 (b) shows the error bound convergence (the difference between the two approximations). The hypothetical mechanism is said to have a large number of layers, with the parameters of the 6 outermost known. To show that the theorems still hold even if the mechanism is constructed haphazardly, two-port network immittance parameters were chosen randomly for each of the 6 layers with $^k s_1 \in (0, 18)$, $^k s_2 \in (0, 27)$, and $^k s_3 \in (0, \min[\sqrt{^k s_1 \, ^k s_2}, 16])$. The restriction on $^k s_3$ ensure that the immittance matrix is positive definite and physically consistent. Other trials perform similarly.

The lumped stiffness of the remaining unconsidered layers will be in the interval $[0, \infty)$. x_j represents the stiffness of the actuator when this lumped stiffness for the remaining layers is zero. y_j represents the stiffness of the actuator when this lumped stiffness for the remaining layers is infinite. For a finite nonzero compliance, the stiffness of the overall actuator should be between the values of x_j and y_j. Since these are

the same in the limit, then the compliance of the innermost layers have a negligible effect on the overall stiffness of the passive actuator for actuators with many layers.

VIII. EXPERIMENTAL EVALUATION OF STIFFNESS CONVERGENTS

The example shown in Figure 8 is meant to show that the theorems in section VI apply *any* conceivable actuator, even if the choice of immittances is random or in a range that would never be selected in practice. In order to see how these theorems apply to a useful engineering situation, we will examine the convergents for the 3-layer actuator used to drive the biologically inspired camera positioning device. The application, as well as how the geometry of each layer was chosen is described in [3]. The immittance parameters for each rhomboidal strain amplification mechanism were determined from the geometry using the method in [22]. These can be used to calculate the convergents.

The convergents can then be measured using a collection of experiments. To measure y_0, we take the third layer alone, as it is the outermost layer. The third layer is fixed in the input direction as shown in Figure 9. The output position is varied using an NAI aperture micropositioning stage, and the force is recorded using a Futek LSB200 load cell with a 1 N range. y_0 was determined from a linear fit to the force-displacement data. Because the input was fixed, the experiment is really recording the stiffness of half the rhomboidal mechanism. Therefore, the mechanism was inverted and the procedure repeated.

To measure x_0, a similar procedure was used, shown in Figure 10. This time the input is free to contract along the major axis (input) as the minor (output) axis extends. x_0 was recorded from a linear fit to the force-displacement data.

To measure y_1, the second layer was installed within the third layer, and a steel block was installed along the input axis of each rhomboid in the second layer, as shown in Figure 11. The steel block can be considered to be rigid compared to the rhomboidal mechanisms. The output of the third layer was
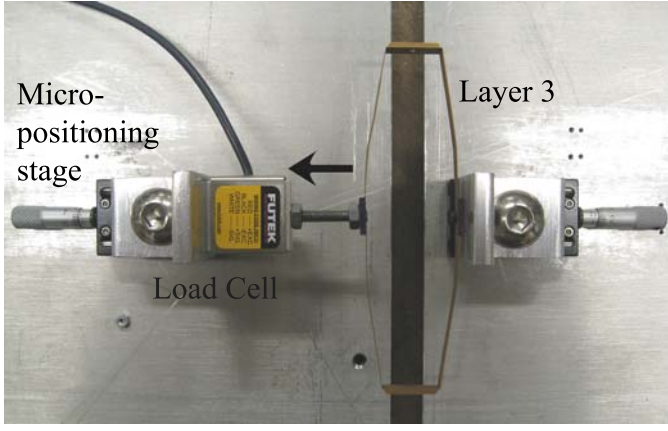
Fig. 10. Experimental evaluation of x_0 (input-free stiffness of the outermost layer only)
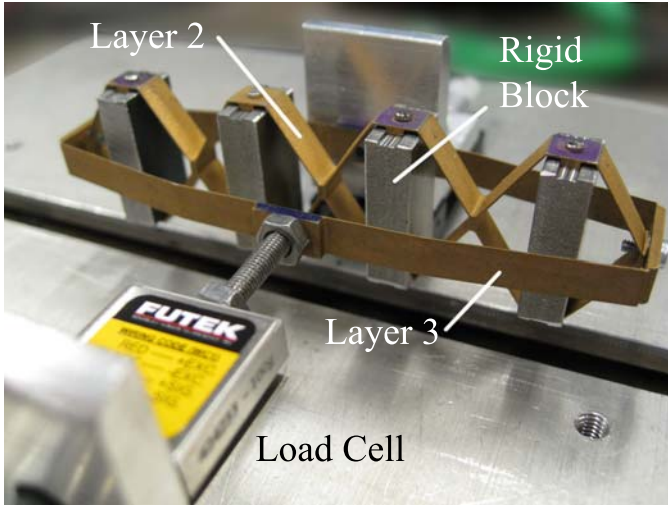

Fig. 11. Experimental evaluation of y_1 (input-fixed stiffness of the outermost two layers). Steel blocks are used to prevent motion of the second layer in the input direction. The evaluation of x_1 (input-free stiffness of the outermost two layers) is similar, but with the rigid blocks removed. The lumped stiffness of the entire mechanism, or $y_2 = x_2$, is also measured in a similar way, but the mechanism is replaced with the full actuator shown in Figure 4.

extended using the micropositioning stage as in the previous experiments. x_1 was determined using the same setup, but with the blocks removed. Both were determined from linear fits to the force-displacement data.

The first layer is the strain amplifying mechanism incorporated into the APA50XS, and there is no way to test it independently without damage. Cédrat also tabulates the blocked force and stiffness for the entire part, not separately for the piezoelectric stack and compliant mechanism. Therefore, we consider the continued fraction to terminate here, and x_2, y_2 and the lumped stiffness are synonymous. This value is equal to F^{block}/δ^{free}. Since F^{block} and δ^{free} are important in their own right, we conducted experiments to determine these quantities separately and have used their values to determine the lumped stiffness value. The experimental results and analytical predictions are shown in Figure 12. Manufacturer-provided values of the APA50XS units and the theoretical values of the second and third layer strain amplifier immittances can be

TABLE I
PIEZOELECTRIC CELLULAR ACTUATOR PARAMETERS

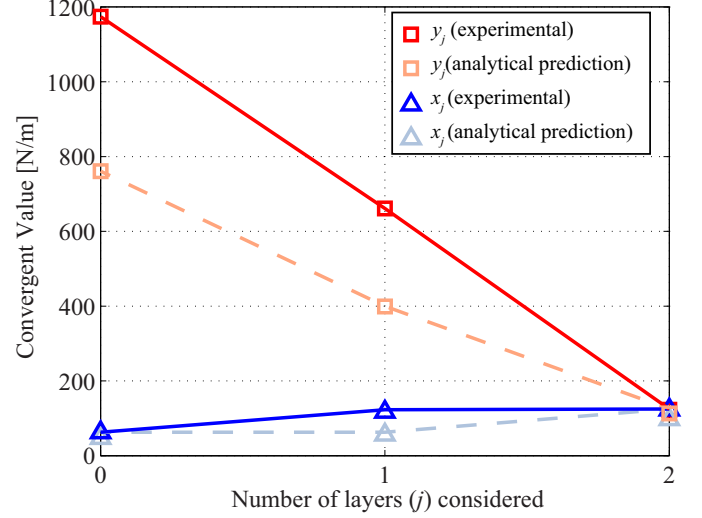| Quantity	Value	Unit
Cédrat APA50XS Parameters		
Stiffness	230e3	N/m
Free Displacement	78	μ m
Blocked Force	18	N
Second and Third Layer Immittances		
$^2s_1$	756e3	N/m
$^2s_2$	424e3	N/m
$^2s_3$	562e3	N/m
$^3s_1$	113e3	N/m
$^3s_2$	761	N/m
$^3s_3$	8.90e3	N/m

Fig. 12. Measured and theoretical stiffness convergents for a 3 layer cellular actuator

found in Table VIII. Recall that the first and second layers each contain 4 units in series and will have 1/4 of the lumped stiffness of a single unit.

The error between the theoretical and experimental values shown in Figure 12 stems primarily from differences between the theoretical and actual values of the immittances of the strain amplifying mechanisms themselves. This is particularly true for the third layer, since it is extremely thin compared to its overall size, and made using a pryping manufacturing process, leaving it vulnerable to residual stresses and other artifacts. This is discussed further in the author's prior work [22]. In addition, the force sensors have some compliance, which may have affected the result. Although care was taken with the alignment of the strain amplification mechanisms during the experiment, a certain amount of misalignment and internal preloading was unavoidable, which may have made the mechanism appear stiffer than the model would predict. Finally, the motion of the stage changes the angle slightly, and this change in angle is a nonlinearity not captured by the model. Despite the fact that the individual values themselves vary due to manufacturing inaccuracies and misalignments in the setup, it is clear that the sequences x_j and y_j are monotonically increasing and monotonically decreasing, respectively, and that they converge to the same limit. Therefore, the consequences of the theorems are borne out in real engineering
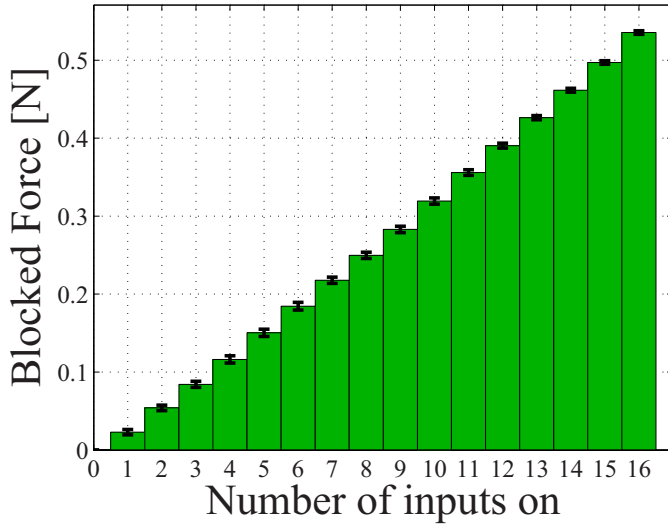
Fig. 13. Blocked force measurements with activation. Error bars are 1 standard deviation.

Fig. 14. Free displacement experiment

situations.

IX. BLOCKED FORCE AND FREE DISPLACEMENT MEASUREMENTS

In addition to verifying the stiffness of the actuator, the blocked force and free displacement were evaluated on the complete actuator prototype. The goal was to see not only how closely the actuator matched the predicted values based on the model, but also to see how repeatable the force and displacement values at the output are when different combinations of piezoelectric stacks are activated.

The experiment to measure the blocked force is similar to that shown in Figure 11, however, instead of the second and third layer units with rigid blocks, it uses the full actuator shown in Figure 4. Each piezoelectric stack is activated one at a time. The output is held stationary. The force at the output is measured and recorded using the Futek load cell for each level of activation. When all inputs have been activated, they are deactivated one by one and the forces recorded. 16 trials were conducted, with an arbitrary activation/deactivation order each time. The results are shown in Figure 13. Figure 13 shows that the force profile is quite linear and very repeatable regardless of the order in which the piezoelectric stacks are activated. Although the maximum blocked force is only 59% of the 0.907 N predicted by the model [3], it shows there is enough fidelity for the model to be useful in generating the first iteration of a nested multilayer actuator design. We expect that agreement with the model will be better for less aggressive force/displacement tradeoffs and will improve with better manufacturing and assembly techniques.

The free displacement of the actuator is measured using the setup shown in Figure 14. Due to the weight of the piezoelectric stacks and the low out of plane rigidity of the third layer, there will be significant deflection if the actuator is suspended from one end. For this reason the actuator is clamped at its centroid and both mounting flanges are allowed to exte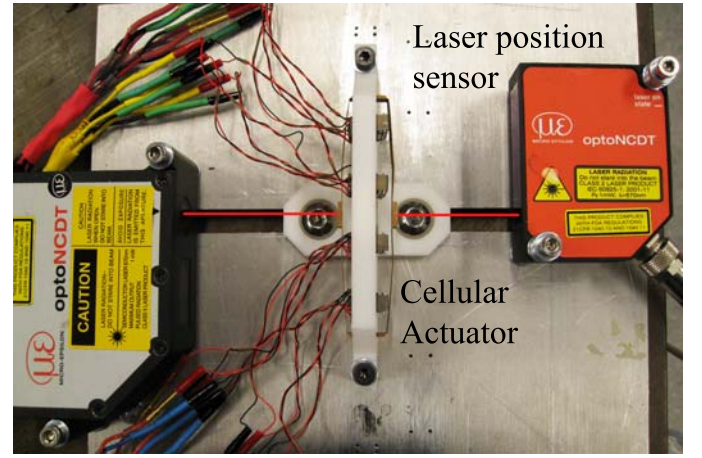nd outward as piezoelectric stacks are activated. The piezoelectric stacks are activated one by one as in the blocked force experiment. The position of each output flange is sensed by a micro-epsilon optoNCDT laser positioning sensor with a range of 20 mm. The two measurements are summed to determine the free displacement. Results are shown in Figure 15.

As with the blocked force, the free displacement predicted by the analytical model (8 mm) is higher than that observed in the experiment. The model only reaches 41% of the theoretical prediction. This is likely because of losses due to deformation in the adhesive holding the first layer units together in series. This is expected to be closer to the theoretical value once these are replaced with monolithic sets of 4 manufactured in one piece. The repeatability of the free displacement is also very good. The linearity is good through the activation of the first 8 units. Beyond this there is a visible reduction in the amount of displacement per unit activated. This is due to a saturation effect; as the actuator contracts, the angle in the deformed configuration approaches zero and the rhomboid approaches a rectangle. This effect is not captured by the linear model. Because this actuator is designed to be used in an antagonistic configuration, as described in section V its extension will only be in the first half of its range. For comparison, a trendline based on activation of the first 8 inputs has been added to Figure 15. The dashed portion shows the line extrapolated to show the "effective free displacement." Using the effective figure, the displacement reaches 50% of the theoretical value. In actuators designed to be used in a single-ended configuration, this saturation effect will be less pronounced.

X. DISCRETE SWITCHING VIBRATION SUPPRESSION FOR VIBRATION-FREE POINT-TO-POINT MOTION

Since the actuators of the camera positioner have 16 inputs/side, it represents the highly discretized redundant actuation paradigm described in [7]. Because of the flexible nature of the actuators, it will naturally have an oscillatory response when inputs are activated. However, if the natural frequencies of the resonant modes are known, nearly vibration-free moves can be made by carefully choosing the switch times
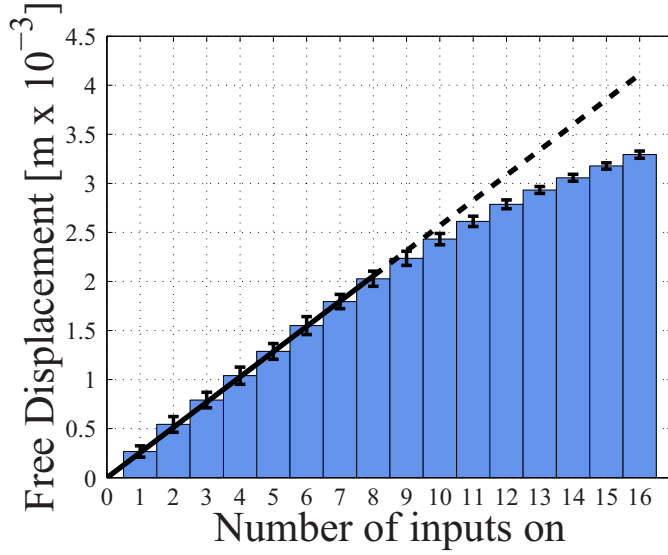
Fig. 15. Free displacement measurements with activation. Error bars are 1 standard deviation.

of each input, a method know as minimum switching discrete switching vibration suppression (MSDSVS) [7]. This section describes how this was implemented and presents results.

A. Natural vibrational modes of the camera positioner

The natural frequencies of oscillation of the camera positioner were determined using simple experiments. The 16 piezoelectric inputs on one side were excited by a swept sinusoidal signal, generated by an Agilent function generator, which was amplified by a Cédrat CA45 linear amplifier. The opposite side was not energized. The amplitude was read in the time domain during the sweep and the maximum amplitude was noted to be at 9.9 Hz. Since the natural frequencies were low, the residues and damping values are not required for MSDSVS, and the change in amplitude was distinct enough to resolve the resonant frequency to an accuracy of 0.1 Hz, this very simple experiment is sufficient.

Surprisingly, the amplitude of oscillation of any remaining modes was insignificant relative to the amplitude of vibration of the first mode. Therefore, for satisfactory operation of the camera positioning mechanism, it is only necessary to suppress a single mode, greatly simplifying the determination and implementation of appropriate MSDSVS commands.

B. Experimental evaluation

Camera positioner firmware and a user interface are implemented in National Instruments LabView software. The system uses NI cRIO-9024 real-time control hardware with an NI 9401 module with a 100ns resolution installed and a custom high voltage switching circuit [7]. The user specifies the desired position and the system will select and initiate an MSDSVS move based on the current position. Details of how the MSDSVS pulses are computed can be found in the Appendix and [26].

For accurate recording, the position is measured by a Midori Orange Pot CP-30H (hall effect variable resistor).
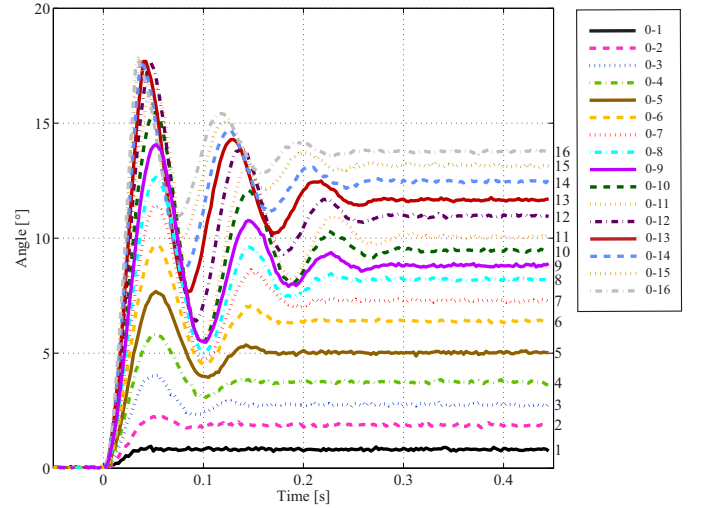

Fig. 16. Step response of the biologically inspired camera positioner. Curves shown for a single direction, center to all 16 positions shown. Steady state position is indicated to the right.
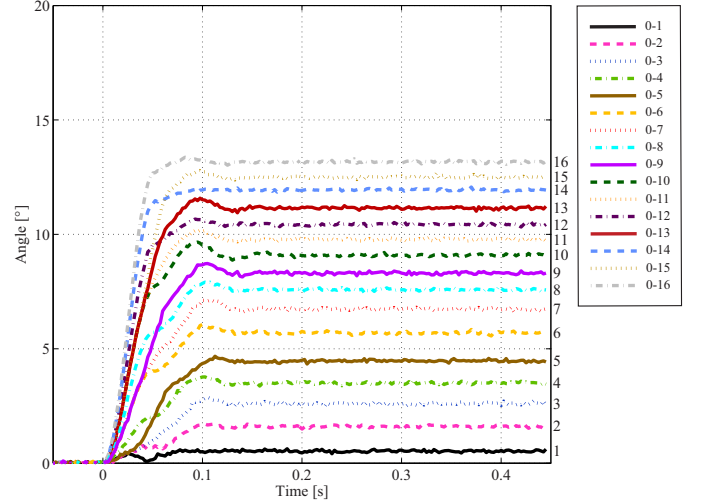

Fig. 17. Minimum switching discrete switching vibration suppression response of the biologically inspired camera positioner. Curves shown for a single direction, center to all 16 positions shown. Steady state position is indicated to the right.

In applications such as autonomous vehicle navigation, the camera angle could be determined using salient features in the image, and once calibrated, the potentiometer could be removed. Because MSDSVS is an open-loop method, this feedback is not necessary for control.

C. Results

Figure 16 shows the step response of the camera positioner. It is evident that the device is lightly damped from the large overshoot, particularly for the longer moves. Locations 13-16 also show a saturation effect; most likely the overshoot causes the output flange to collide with the first layer units. This is due to the overshoot; quasistatic motions produce no collisions.

Figure 17 shows the response to the various MSDSVS patterns for each of the 16 discrete positions. The resulting responses have low overshoot, or none at all. The response reaches steady state within 0.14 s. The improvement in per-

formance is evident in the companion video. Therefore this method is effective in suppressing vibration. The performance of the algorithm on the camera positioner is better than the simple setup in [7], giving credence to the conjecture therein that the algorithm would cancel oscillation better on engineering devices with lower and more well-known natural frequencies.

D. Discussion

Figure 16 shows that there are some nonlinearities in the camera positioner system dynamics. This is primarily due to variation in frequency with actuator length. However, despite these nonlinear effects, the MSDSVS commands based on the simple linear model of the system are effective for the range of motion of this device. For long serial chains of actuators such as these, some more advanced or heuristic methods may be necessary to mitigate the change in natural frequency with length.

Although MSDSVS is useful for quickly reorienting the gaze axis of the camera (saccades) and canceling oscillation generated by the command itself, a feedback control method will be necessary for smoothly following objects through the field of view and canceling oscillation produced by unmodeled disturbances. The mode identified this section is well below the sampling frequency of the camera, but future designs with less damping, more degrees of freedom and larger displacements may have modes of vibration that have natural frequencies above the sampling rate. In these cases, a feedback technique called intersample discretization [27], may be effective. It uses carefully coordinated switches among the actuator's allowable discrete values during a discrete time sample in place of a zero order hold to suppress high frequency oscillations.

XI. CONCLUSION

In an effort to increase the strain rate of amplified piezoelectric stack actuators, researchers have considered using multiple stages of amplification, the output of each of which is the input to the next. This work establishes a mathematical framework that connects the stiffness properties of the entire actuators to the properties of each individual stage. This culminates in two theorems which show that the stiffness can be approximated simply by considering the outermost layers in the nested configuration. A principled procedure for the design of these mechanisms, which follows directly from these results, was used to construct a camera positioner with actuation inspired by human recti muscles. Experimental results from the camera positioner confirm the mathematical trends.

Because each stage in the hierarchy contains several instances of the lower-level subunits, the numerous individual segments of active material give the resulting actuator a cellular structure similar to human muscle. This highly discretized on-off actuation paradigm in combination with the inherent compliance gives rise to oscillatory behavior. By applying the minimum switching discrete switching vibration suppression technique to the camera positioner, visible reductions amplitude and duration of these oscillations is observed. This technique only suppresses oscillation arising from the command itself; it will not suppress oscillation due to external disturbances. As camera positioners move in free space, this is good enough for numerous applications.

Future work may involve further optimization of the sequence of layer geometries, performance comparisons among actuators with various numbers of layers, and frequency domain modeling of actuators of this type. In addition, it will explore feedback control strategies with discretized inputs like those in MSDSVS, but with the ability to suppress external oscillations.

APPENDIX
DETERMINATION OF MSDSVS SWITCHING PATTERNS

Since the plant has only one natural frequency that needs to be suppressed, vibration suppression can be achieved using only 3 impulses. Given a set of amplitudes, the timings can be calculated analytically using the following formulas, obtained by setting the sum of the effects of all impulses to be equal to zero in the complex plane. With a single mode, this results in:

$$\phi_1 = \arccos \frac{A_2^2 - A_0^2 - A_1^2}{2A_1 A_0} \tag{31}$$

$$\phi_2 = \arcsin -\frac{A_1 \sin \phi_1}{A_2} \tag{32}$$

where $A_i \in \mathbf{D} \subset \mathbb{Z}$ are the integer amplitudes applied to the camera positioner and ϕ_i represent the phase delay of impulse i with respect to the resonant frequency. Requiring that

$$\frac{A_2^2 - A_0^2 - A_1^2}{2A_1 A_0} \in [\, -1, \, 1 \,] \tag{33}$$

and

$$\frac{A_1 \sin \phi_1}{A_2} \in [\, -1, \, 1 \,] \tag{34}$$

(so that all $\phi_i \in \mathbb{R}$) defines the allowable set of amplitudes for which a vibration-free point-to-point move is possible.

Because (31,32) are analytical expressions, a solution is guaranteed, provided that the relative magnitudes of the impulses result in arguments in the domain of the inverse trigonometric functions. This means that a monotonic "staircase" solution is always possible for a single frequency for move distances greater than 1. However, it is simpler to compute the solution graphically than to use (31) and (32). Representing the impulses as vectors in $\mathbb{C}$, the first impulse corresponds to a vector directed along the positive real axis. For even numbered distances, a vibration free move can be computed that includes two impulses of equal amplitude, one along the positive real axis and the other along the negative real axis. This is equivalent to a ZV shaper [28] applied to a step input. For odd numbered move distances, the command can be computed as follows:

1) Decompose the move distance y_g into $y_g = q + p$, where q is even and p is odd. p and q must be chosen such that (33) and (34) are satisfied.
2) Set the first amplitude, $A_0 = p$. This lies along the positive real axis.
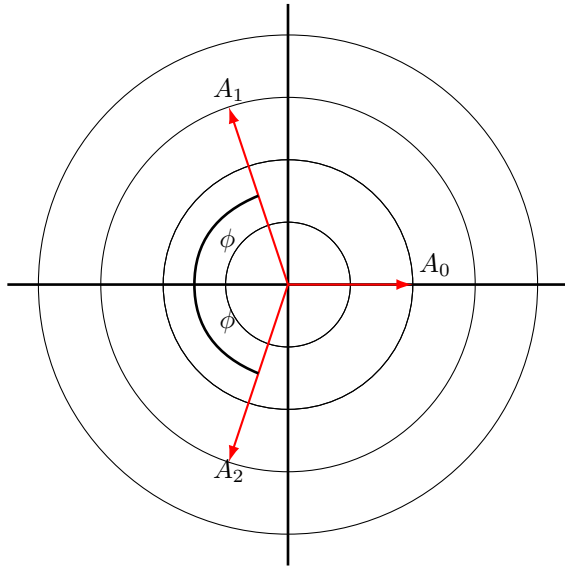
Fig. 18. Representation of impulses in the complex plane for an odd number of impulses

TABLE II
MSDSVS PATTERNS FOR THE BIOLOGICALLY INSPIRED CAMERA
POSITIONING MECHANISM

move distance	A_0	A_1	A_2	ϕ_1	ϕ_2
Units Activated				°	
1	1	-1	1	60	120
2	1	1	n/a	180	n/a
3	1	1	1	120	240
4	2	2	n/a	180	n/a
5	1	2	2	104.47	255.52
6	3	3	n/a	180	n/a
7	3	2	2	138.59	221.41
8	4	4	n/a	180	n/a
9	3	3	3	120	240
10	5	5	n/a	180	n/a
11	5	3	3	146.44	213.56
12	6	6	n/a	180	n/a
13	5	4	4	128.68	231.31
14	7	7	n/a	180	n/a
15	5	5	5	120	240
16	8	8	n/a	180	n/a

3) Set the two remaining amplitudes $A_1 = A_2 = q/2$.
4) A_1 and A_2 will be represented as vectors of equal magnitude in the complex plane, at an angle ϕ above and below the negative real axis.
5) Solve for the ϕ that gives a vector sum of zero.

Figure 18 illustrates the phasors in the complex plane for an odd-numbered move. The MSDSVS patterns computed using this method are listed in Table II. When multiple solutions were found, the one that could be completed in minimum time was chosen. Phases can be converted to timings using the natural frequency of 9.9 Hz.

ACKNOWLEDGMENT

REFERENCES

[1] I. M. Koo, K. Jung, J. C. Koo, J.-D. Nam, Y. K. Lee, and H. R. Choi, "Development of a soft-actuator-based wearable tactile display," *IEEE Transactions on Robotics*, vol. 24, no. 3, pp. 549–558, June 2008.

[2] N. Tsagarakis and D. G. Caldwell, "Development and control of a soft-actuated exoskeleton for use in physiotherapy and training," *Autonomous Robotics*, vol. 15, no. 1, pp. 21–33, 2003.

[3] J. Schultz and J. Ueda, "A Camera Positioner Driven by Muscle-Like Actuation," in *Proceedings of the IEEE International Conference on Biomedical Robotics & Biomechatronics (BioRob)*, Roma, Italy, 2012.

[4] J. Ueda, *Advanced Mechatronics and MEMS Devices*, ser. Microsystems, D. Zhang, Ed. SpringerLink, 2013, vol. 23.

[5] J. D. Enderle and J. W. Wolfe, "Time-optimal control of saccadic eye movements," *IEEE Transactions on Biomedical Engineering*, vol. BME-34, no. 1, pp. 43–55, January 1987.

[6] J. Schultz and J. Ueda, "Analysis of antagonist stiffness for nested compliant mechanisms in agonist-antagonist arrangements," in *Proceedings of the ASME Dynamic Systems and Controls Conference*. Arlington, VA: ASME Dynamic Systems and Control Division, November 2011.

[7] ——, "Experimental verification of discrete switching vibration suppression," *Mechatronics, IEEE/ASME Transactions on*, vol. 17, no. 2, pp. 298 –308, April 2012.

[8] T. Villgrattner and H. Ulbrich, "Design and control of a compact high-dynamic camera-orientation system," *IEEE/ASME Transactions on Mechatronics*, vol. 16, no. 2, pp. 221–231, April 2011.

[9] Y.-C. Lee, C.-C. Lan, C.-Y. Chu, C.-M. Lai, and Y.-J. Chen, "A pan-tilt orienting mechanism with parallel axes of flexural actuation," *ASME/IEEE Transactions on Mechatronics*, vol. 18, no. 3, pp. 1100–1112, 2013.

[10] S.-C. Huang and W.-L. Chen, "Design of topologically optimal microgripper," in *IEEE International Conference on Systems, Man and Cybernetics*, 2008.

[11] S. Kota, K.-J. Lu, Z. Kreiner, B. Trease, J. Arenas, and J. Geiger, "Design and application of compliant mechanisms for surgical tools," *ASME Journal of Biomedical Engineering*, vol. 127, pp. 981–989, November 2005.

[12] K. Uchino, *Piezoelectric Actuators and Ultrasonic Motors*, ser. Electronic Materials: Science and Technology, H. L. Tuller, Ed. Kluwer Academic Publishers, 1997.

[13] J. Paros and L. Weisbord, "How to design flexure hinges," *Machine Design*, vol. 37, no. 27, pp. 151–156, November 1965.

[14] N. Lobontiu and E. Garcia, "Analytical model of displacement amplification and stiffness optimization for a class of flexure-based compliant mechanisms," *Computers & Structures*, vol. 81, no. 32, pp. 2797–2810, 2003.

[15] J. Ueda, T. Secord, and H. Asada., "Large effective-strain piezoelectric actuators using nested cellular architecture with exponential strain amplification mechanisms," *IEEE/ASME Transactions on Mechatronics*, vol. 15, pp. 770–782, 2010.

[16] J. H. Kim, S. H. Kim, and Y. K. Kwak, "Development of a piezoelectric actuator using a three-dimensional bridge-type hinge mechanism," *American Institute of Physics Review of Scientific Instruments*, vol. 74, no. 5, pp. 2918–2924, May 2003.

[17] T. Secord and H. Asada, "A variable stiffness pzt actuator having tunable resonant frequencies," *Robotics, IEEE Transactions on*, vol. 26, no. 6, pp. 993 –1005, dec. 2010.

[18] E. E. Steltz, "Redesign of the micromechanical flying insect in a power density context," Ph.D. dissertation, University of California, Berkeley, May 2008.

[19] D. C. T. Ruete, "Ocular physiology," *Strabismus*, vol. 7, no. 1, pp. 43–60, January 1999.

[20] J. Choma, Jr., *Electrical Networks: Theory and Analysis*. New York: John Wiley and Sons, Inc., 1985.

[21] M. Abdalla, M. Frecker, Z. Gürdal, T. Johnson, and D. K. Lindner, "Design of a piezoelectric actuator and compliant mechanism combination for maximum energy efficiency," *Institute of Physics Smart Materials and Structures*, vol. 14, pp. 1421–1430, November 2005.

[22] J. Schultz and J. Ueda, "Two-port network models for compliant rhomboidal strain amplifiers," *IEEE Transactions on Robotics*, vol. 29, no. 1, pp. 42–54, February 2013.

[23] W. B. Jones and W. Thron, *Continued Fractions: Analytic Theory and Applications*, ser. Encyclopedia of Mathematics and its Applications, G.-C. Rota, Ed. Addison-Wesley, 1980, vol. 11.

[24] A. M. Rockett and P. Szüz, *Continued Fractions:*. World Scientific, 1992.

[25] E. Zakon, *Mathematical Analysis I*, J. Spiegelman, Ed. The Trilla Group, 1975.

[26] J. Schultz, "Mathematical modeling and control of a piezoelectric cellular actuator exhibiting quantization and flexibility." Ph.D. dissertation, Georgia Institute of Technology, December 2012.

[27] J. Schultz and J. Ueda, "Intersample discretization of control inputs for flexible systems with quantized cellular actuation," in *Proceedings of the ASME Dynamic Systems and Controls Conference*, Cambridge, MA, September 2010.

[28] N. C. Singer and W. P. Seering, "Preshaping command inputs to reduce system vibration," *ASME Journal of Dynamic Systems, Measurement, and Control*, vol. 112, pp. 76–82, 1990.